CCFE
CULHAM CENTRE FOR FUSION ENERGY

UK Atomic Energy Authority

UKAEA-CCFE-PR(22)87

S. Saarelma, J.W. Connor, P. Bilkova, P. Bohm, A.R. Field, L. Frassinetti, R. Fridstrom A. Kirk, JET Contributors*

Testing a Prediction Model for the H-mode Density Pedestal against JET-ILW Pedestals

Testing a Prediction Model for the H-mode Density Pedestal against JET-ILW Pedestals

S. Saarelma, J.W. Connor, P. Bilkova, P. Bohm, A.R. Field, L. Frassinetti, R. Fridstrom A. Kirk, JET Contributors*

This is a preprint of a paper submitted for publication in Nuclear Fusion

Testing a Prediction Model for the H-mode Density Pedestal against JET-ILW Pedestals

S. Saarelma[1], J.W. Connor[1], P. Bilkova[2], P. Bohm[2], A.R. Field[1], L. Frassinetti[3], R. Fridstrom[3] A. Kirk[1] and JET Contributors*

[1]United Kingdom Atomic Energy Authority, Culham Centre for Fusion Energy, Culham Science Centre, Abingdon OX14 3DB, United Kingdom

[2]Institute of Plasma Physics of the CAS, Za Slovankou 3, 182 00 Prague 8, Czech Republic

[3]Division of Fusion Plasma Physics, KTH Royal Institute of Technology, Stockholm SE-100 44, Sweden

** See the author list of 'Overview of JET results for optimising ITER operation' by J. Mailloux et al 2022 Nucl. Fusion 62 042026*

Abstract

The neutral ionisation model proposed by R J Groebner et al. (Phys Plasmas **9** 2134 (2002)) to determine the plasma density profile in the H-mode pedestal, extended to include charge exchange processes in the pedestal stimulated by the ideas of Mahdavi et al. ((Phys Plasmas **10** 3984 (2003)). The model is then tested against JET H-mode pedestal data, both in a 'standalone' version using experimental temperature profiles and also by incorporating it in the Europed version of EPED. The model is able to predict the density pedestal over a wide range of conditions with good accuracy. It is also able to predict the experimentally observed isotope effect on the density pedestal that eludes simpler neutral ionization models.

1. Introduction

Core energy confinement in tokamaks operating in H-mode is sensitive to the properties of the associated edge pedestal. Specifically, the limiting core temperature profile is believed to be

'stiff', i.e., determined by marginal stability to ion temperature gradient modes [1]. Consequently, it is largely controlled by the boundary condition on the temperature at the top of the H-mode temperature pedestal. Thus, a reliable model for this pedestal is a key requirement for predicting the performance of burning plasma designs, such as ITER or the proposed spherical tokamak STEP.

The EPED model [2] based on the requirement that the pedestal plasma pressure profile is stable to both kinetic ballooning modes (KBMs) and peeling-ballooning modes [3] is often invoked for this purpose. The former is used to set the pressure gradient and the latter to provide the width of the pedestal, together yielding the pressure at the pedestal top. However, one really needs individual models for the profiles of the pedestal ion and electron temperatures, T_i and T_e, respectively, and the plasma density profiles, n_e. There is support from JET for a model for the electron temperature profile in the pedestal based on transport due to electron temperature gradient (ETG) turbulence [4] but this depends strongly on the profile of the parameter $\eta_e = d(\ln T_e)/d(\ln n_e)$: hence one also needs a prescription for the electron density profile to complete this model. This has usually been taken as an experimental input, but some success has been obtained with a theoretically based transport model invoking the source provided by ionisation of neutral particles incident from the scrape-off layer (SOL), together with a pedestal diffusion coefficient, D_{ped} [5, 6]. This could be related to the same ETG turbulence [7] and/or to kinetic ballooning modes (KBM) [8]. Finally, to complete the picture one can appeal to KBM, a combination of ion temperature gradient (ITG) and trapped electron modes (TEM) or ion neoclassical transport (NC) to furnish a model for the pedestal ion temperature profile [8].

The neutral ionisation model described in Ref.5, which considers the ionisation of the incident low energy, Franck-Condon neutrals produced by recycling and gas-puffing incident at the separatrix, has

been tested against experimental data from DIII-D [5], MAST [9] and JET [10]. The enhanced version presented in Ref. 6 includes the effects of the incident higher energy, charge-exchange population generated in the SOL which penetrate further into the plasma column. In this work we use similar ideas to provide a simple model for the effect of charge-exchange processes in the pedestal region.

The ionisation model is described in Section 2, while in Section 3 it is used with experimental temperature profiles to compare with JET data, which we refer to as the 'stand-alone' version. In Section 4 the ionisation model is introduced into the EPED model in the Europed code to compare with experimental data from JET. Section 5 investigates the predictions of the model regarding the isotope effect. Section 6 provides a summary and discussion with some conclusions.

2. The ionisation model for the density profile

2.1. Transport Equations

In the spirit of Ref. 6, which develops the model in Ref. 5 further, we obtain the radial profile of the electron density, $n_e(r)$, in the H-mode pedestal region by balancing radial diffusion, with coefficient $D_{ped}(r)$, against ionisation by both low energy Franck-Condon and more energetic charge exchange neutrals, with densities $n_{FC}(r)$ and $n_{CX}(r)$, respectively, themselves being modelled by balancing inward convection against ionisation and charge exchange sources and sinks.

We use straight field line coordinates: r, θ, φ, with Jacobian $J = rR^2/R_0$, where R is the major radius, its value on the magnetic axis being R_0, the 'minor radius' co-ordinate r is a flux surface label and θ and φ are poloidal and toroidal angles, respectively. In the narrow

pedestal region, we introduce the radial co-ordinate, $x = r - r_{sep}$, where r_{sep} is the radius of the separatrix flux surface, and $r \cong r_{sep}$.

The ionisation model described above is represented by the three equations:

$$\nabla.\left(D_{ped}\nabla n_e\right) = -n_e(\, n_{FC} + n_{CX})S_i \quad (1)$$

$$\nabla.\,(V_{FC}n_{FC}) = -n_e(\, n_{FC}S_i + n_{FC}S_{CX}) \quad (2)$$

$$\nabla.\left((V_{CX}n_{CX})\right) = -n_e\left(\, n_{CX}S_i - \tfrac{1}{2}n_{FC}S_{CX}\right) \quad (3)$$

Introducing the straight field line co-ordinates and averaging over the poloidal angle θ,

$$\frac{d}{dx}\left(D_{ped}\oint R^2|\nabla r|^2 d\theta\,\frac{dn_e}{dx}\right) = -n_e\oint R^2 d\theta\,(\, n_{FC} + n_{CX})S_i \quad (4)$$

$$\frac{d}{dx}\left(\oint R^2|\nabla r|^2 d\theta\, V_{FC,r}\, n_{FC}\right) = -n_e\oint R^2 d\theta\,(\, n_{FC}S_i + n_{FC}S_{CX}) \quad (5)$$

$$\frac{d}{dx}\left(\oint R^2|\nabla r|^2 d\theta\, V_{CX,r}n_{CX}\right) = -n_e\oint R^2 d\theta\left(n_{CX}S_i - \tfrac{1}{2}n_{FC}S_{CX}\right), \quad (6)$$

where S_i and S_{CX} are the ionisation and charge exchange rates, respectively, while $V_{FC,r}$ and $V_{CX,r}$ are the corresponding radial velocities of the two species, each considered to be mono-energetic. Thus, $S_i = \sigma_i V_{th,e}$, $S_{CX} = \sigma_{CX}V_{th,i}$, where $\sigma_{i,CX}$, are the corresponding cross-sections, which will vary with electron and ion temperatures, and $V_{th,e}$ and $V_{th,i}$ are the electron and ion thermal speeds respectively. For the radial velocities of the neutrals, we follow Ref. 6, setting $|V_{FC,r}| = \sqrt{8E_{FC}/\pi^2 M_i}$, with $E_{FC} \sim 3\ eV$, and $|V_{CX,r}| = \sqrt{2T_i/\pi M_i}$ (we drop the suffix r, below).

The factor ½ in eqn. (3) represents the fact that the outward flux of fast charge exchange neutrals is taken to be lost. The diffusion coefficient D_{ped} may have a profile dependence arising from dependencies on $T_{e,i}$ and n_e; e.g., gyro-Bohm diffusion produces $D_{ped}{\sim}T_e^{3/2}/B^2L$, where L is some microscopic length and B is the magnetic field; alternatively, it may involve resistivity, as occurs for resistive interchange modes, leading to $D_{ped}{\sim}n_e/T_e^{1/2}B^2$. In the modelling described later, we suppose it arises from a combination of ETG and KBM turbulence.

A similar set of equations were proposed in the SOL in Ref. 6, while those in Ref. 5 follow on neglecting n_{CX}.

It is convenient to introduce a flux surface average over poloidal angle: $\langle A\rangle = \oint R^2 A d\theta \,/\, \oint R^2 d\theta$. To make the system of equations (4)-(6) readily tractable we introduce two form factors:

$$f_{FC} = \langle|\nabla r|^2 n_{FC}\rangle/\langle n_{FC}\rangle\langle|\nabla r|^2\rangle,\ f_{CX} = \langle|\nabla r|^2 n_{CX}\rangle/\langle n_{CX}\rangle\langle|\nabla r|^2\rangle. \quad (7)$$

If the source of the Franck Condon neutrals is localised, say at some angle θ_0, then $f_{FC} \cong R^2(\theta_0)|\nabla r|^2(\theta_0)/\langle|\nabla r|^2\rangle$, whereas the charge exchange scattering may produce a more isotropic distribution of charge exchange neutrals with f_{CX} tending to unity. In general, one needs a numerical simulation of the neutral processes to evaluate these quantities precisely; alternatively, they could be treated as fitting parameters.

2.2. Solution Procedure

Using the expressions (7), eqn. (5) implies

$$n_e S_i \langle n_{FC}\rangle = \frac{|V_{FC}|\, f_{FC}}{(1+S_{CX}/S_i)} \frac{d}{dx}\langle n_{FC}\rangle, \quad (8)$$

while combining this result with eqn. (6) yields

$$n_e S_i \langle n_{CX}\rangle = |V_{CX}| f_{CX} \frac{d}{dx}\langle n_{CX}\rangle + \frac{|V_{FC}| f_{FC} S_{CX}}{2(S_i+S_{CX})} \frac{d}{dx}\langle n_{FC}\rangle \quad (9)$$

Inserting these two results into eqn. (4) and integrating once, we obtain

$$\langle|\nabla r|^2\rangle D_{ped}\frac{dn_e}{dx} = -\frac{\left(1+\frac{S_{CX}}{2S_i}\right)}{\left(1+\frac{S_{CX}}{S_i}\right)}|V_{FC}|f_{FC}\langle n_{FC}\rangle - |V_{CX}|f_{CX}\langle n_{CX}\rangle + C. \quad (10)$$

Here $C = \langle|\nabla r|^2\rangle D_{ped}\frac{dn_e}{dx}|_{x=-\infty}$ is a constant of integration that is determined by the condition that deep into the plasma, both neutral densities should vanish. It is to be remarked that in Ref. 5, C was arbitrarily set to zero, whereas we now allow the more realistic finite density gradient inboard of the pedestal.

Equations (4) and (10) provide an expression for $n_{FC}(x)$ in terms of $n_e(x)$:

$$\langle n_{FC}\rangle\left[1-\frac{|V_{FC}|f_{FC}}{|V_{CX}|f_{CX}}\frac{\left(S_i+\frac{S_{CX}}{2}\right)}{(S_i+S_{CX})}\right] = -\frac{1}{n_e S_i}\frac{d}{dx}\left(\langle|\nabla r|^2\rangle D_{ped}\frac{dn_e}{dx}\right) + \frac{1}{|V_{CX}|f_{CX}}D_{ped}\frac{dn_e}{dx} - \frac{C}{|V_{CX}|f_{CX}\langle|\nabla r|^2\rangle} \quad (11)$$

and then $n_{CX}(x)$ follows from eqn. (9). The electron density profile is then given by the third order equation

$$\frac{d}{dx}\left(L_2(n_e)\right) = \frac{n_e S_i}{|V_{FC}|}\left(1+\frac{S_{CX}}{S_i}\right)L_2(n_e), \quad (12)$$

where the non-linear, second order operator $L_2(n_e)$ is defined by:

$$\left[1-\frac{|V_{FC}|f_{FC}}{|V_{CX}|f_{CX}}\frac{\left(S_i+\frac{S_{CX}}{2}\right)}{(S_i+S_{CX})}\right]L_2(n_e) = -\frac{C}{|V_{CX}|f_{CX}} + \frac{1}{|V_{CX}|f_{CX}}D_{ped}\frac{dn_e}{dx} - \frac{1}{n_e S_i}\frac{d}{dx}\left(\langle|\nabla r|^2\rangle D_{ped}\frac{dn_e}{dx}\right) \quad (13)$$

It may be more convenient to replace this third order equation by an iterative solution based on a second order equation. Using eqn. (10) to replace $n_{CX}(x)$ and introducing the solution of eqn. (8) for $n_{FC}(x)$ yielding

$$\langle n_{FC}\rangle = \langle n_{FC}(0)\rangle \exp\left(\int_0^x dx \frac{n_e(S_i+S_{CX})}{f_{FC}|V_{FC}|}\right) \quad , \tag{14}$$

eqn. (4) becomes

$$\frac{d}{dx}\left(\langle|\nabla r|^2\rangle D_{ped}\frac{dn_e}{dx}\right) = -n_e S_i\left[-D_{ped}\left(\frac{dn_e}{dx} - \frac{dn_e}{dx}|_{x=-\infty}\right) + \left(1 - \frac{|V_{FC}|f_{FC}}{|V_{CX}|f_{CX}}\frac{\left(S_i+\frac{S_{CX}}{2}\right)}{(S_i+S_{CX})}\right)\langle n_{FC}(0)\rangle \exp\left(\int_0^x dx' \frac{n_e(x')(S_i+S_{CX})}{f_{FC}|V_{FC}|}\right)\right] \tag{15}$$

The integral in the last term can be iterated in $n_e(x)$ until one has a self-consistent solution of eqn. (15) for $n_e(x)$. A convenient starting point is the solution of eqn. (4) in the absence of n_{CX}. In this limit, eqn. (4) reduces to

$$\frac{d}{dx}\left(\langle|\nabla r|^2\rangle D_{ped}\frac{dn_e}{dx}\right) = n_e D_{ped}\frac{(S_i+S_{CX})}{|V_{FC}|}\left(\frac{dn_e}{dx} - \frac{dn_e}{dx}|_{x=-\infty}\right) \tag{16}$$

The presence of $\frac{dn_e}{dx}|_{x=-\infty}$ prevents obtaining the analytic solution obtained in [5], so this equation must be solved numerically before inserting its solution in eqn. (15) to begin the iterative process.

However, the form of eqn. (15) obscures how it reduces to the equation derived in Ref 5 when charge exchange neutrals are omitted from the model. This limit is evident if one derives the second order equation for n_e involving n_{CX}, rather than n_{FC} as in eqn. (15):

$$\frac{d}{dx}\left(\langle|\nabla r|^2\rangle D_{ped}\frac{dn_e}{dx}\right) = n_e S_i\left[\frac{(S_i+S_{CX})}{(S_i+S_{CX}/2)}\frac{\langle|\nabla r|^2\rangle D_{ped}}{|V_{FC}|f_{FC}}\frac{dn_e}{dx} - \frac{(S_i+S_{CX})}{\left(S_i+\frac{S_{CX}}{2}\right)}\frac{C}{|V_{FC}|f_{FC}} + \left(\frac{(S_i+S_{CX})}{(S_i+S_{CX}/2)}\frac{|V_{CX}|f_{CX}}{|V_{FC}|f_{FC}} - 1\right)\langle n_{CX}\rangle\right] . \tag{17}$$

Here the charge exchange neutral density, $\langle n_{CX}\rangle$, is given in terms of $\langle n_{FC}\rangle$ by the solution of eqn. (9):

$$\langle n_{CX}\rangle = \langle n_{CX}(0)\rangle \exp\left(\int_0^x dx' \frac{n_e(x')S_i}{\lceil V_{CX}\rceil f_{CX}}\right) + \frac{|V_{FC}|f_{FC}S_{CX}\langle n_{FC}(0)\rangle}{2\lceil V_{CX}\rceil f_{CX}\left(S_i+S_{CX}-\frac{|V_{FC}|f_{FC}}{\lceil V_{CX}\rceil f_{CX}}S_i\right)}$$

$$\times \left[\exp\left(\int_0^x dx' \frac{n_e(x')S_i}{\lceil V_{CX}\rceil f_{CX}}\right) - \exp\left(\int_0^x dx' n_e(x') \frac{(S_i+S_{CX})}{|V_{FC}|f_{FC}}\right)\right] \quad (18)$$

2.3. Boundary Conditions

The original set of equations, (1) – (3), form a fourth order system requiring four boundary-conditions. Correspondingly, the third-order eqn. (12) naturally requires three boundary-conditions, to be added to that following from the constant of integration, C, i.e., $\frac{dn_e}{dx}|_{x=-\infty}$. Thus, the separatrix values of the electron density, $n_e(0)$, its radial gradient, $\frac{dn_e}{dx}|_{x=0}$ and the Franck-Condon neutrals, $n_{FC}(0)$, would suffice. Alternatively, one could use eqn. (11) to replace $n_{FC}(0)$ by $\frac{d^2n_e}{dx^2}|_{x=0}$, so that all boundary conditions could be expressed in terms of n_e. However, it is more appropriate to remain with the specification of $n_{FC}(0)$ or, equivalently, the incident flux at the separatrix of such neutrals: $\Gamma_{FC} = n_{FC}(0)V_{FC}$. It is of interest that the charge exchange density, and hence $n_{CX}(0)$ specifically, follows directly from eqn. (10).

Reference 6 proposed a simple model for the neutral interactions in the scrape-off layer (SOL) to provide the ratio $w = n_{CX}(0)/n_{FC}(0)$, rather than considering this as an input to the boundary conditions. Furthermore, by considering the SOL region one can also determine $\frac{dn_e}{dx}|_{x=0}$. Thus, the source-free solution for the electron density, where radial diffusion with a diffusion coefficient D_{SOL} is balanced by streaming along the open magnetic field lines on a timescale $\tau_{||}$, follows from the equation

$$D_{SOL}\frac{d^2n_e}{dx^2} = -\frac{n_e}{\tau_{||}}. \quad (19)$$

namely $n_e = n_e(0)\exp\left(-\frac{x}{\sqrt{D_{SOL}\tau_{||}}}\right)$. Thus

$$\frac{dn_e}{dx}|_{x=0} = -\frac{n_e(0)}{\sqrt{D_{SOL}\tau_{||}}}. \quad (20)$$

3. Model results for the JET pedestal database using experimental temperature profiles

The JET database [11] with more than 1000 fitted pedestal profiles of JET plasmas is used to test the model. For the model, we can obtain the boundary conditions $n_{e,sep}$ and $\frac{dn_e}{dx}|_{x=-\infty}$. $\tau_{\|}$ is assumed to be known as well for a given device. We set $\langle n_{FC}(0)\rangle$ to a value of 10^{15} m^{-3} and $\tau_{||}$ = 0.001s but note that the results are to some extent sensitive to these values. Since we have no good model for the poloidal distribution of the neutrals, we set both f_{FC} and f_{CX} to 1, that assumes equal distribution with the poloidal angle. Thus, D_{ped} is the only free parameter to be modelled. In this work we have implemented the model described in Ref.7, where D_{ped} is constructed from three components, the first driven by electron temperature gradient (ETG) turbulence is proportional to the electron heat transport, the second from neoclassical transport and the third driven by kinetic ballooning modes (KBM) is proportional to the extent to which the normalized pressure gradient (α) exceeds the threshold value for kinetic ballooning modes. The ETG part can be calculated from the known heat flux through pedestal and the temperature profile using the normal heat conduction equation:

$$\chi_e = \frac{q_e}{n_e \nabla T}, \quad (21)$$

where $q_e$is the heat flux at the pedestal as calculated from the input heating power and the plasma geometry. The particle transport from ETG is set to be this multiplied by a constant factor $(D_e/\chi_e)_{ETG}$.

Following Ref. 7, the neoclassical part of D_{ped} is taken for simplicity to be

$$D_{e,NC} = \frac{\chi_{e,NC}}{2} = 0.05\left(\frac{\rho_s^2 c_s}{a}\right) \tag{22}$$

Finally, again following Ref.7, the KBM part of diffusion coefficient D_{ped} is assumed to be zero below the KBM stability limit and then increase proportionally to $(\alpha - \alpha_{crit})$, where α is the normalised pressure gradient in the pedestal defined in Ref.12 as

$$\alpha = \frac{2\partial_\psi V}{(2\pi)^2}\left(\frac{V}{2\pi^2 R_0}\right)^{1/2}\mu_0 p'. \tag{23}$$

Here V is the volume enclosed by the flux surface, R_0 is the major radius, p is the pressure and the derivative, represented by $'$, is taken with respect to the poloidal flux ψ and α_{crit} is the stability limit of the KBMs. Since KBMs have a wide radial extent, we assume that the particle transport from them is not local but covers the entire pedestal region. Therefore, instead of a local value of α, we use the average value in the pedestal region. The total D_{ped} from KBM is given by the formula:

$$\begin{cases} C_{KBM}(\alpha - \alpha_{crit}) \cdot \left(\frac{\rho_s^2 c_s}{a}\right), \alpha > \alpha_{crit} \\ 0, \alpha < \alpha_{crit} \end{cases} \tag{24}$$

Using these assumptions, we simulated the entire JET-ILW database using the experimental temperature profile to calculate the ionisation and charge exchange cross-sections, σ_i and σ_{CX}, ∇T, needed in eqn. (21), and α ,needed in eqn. (23) (α is calculating by scaling the value in a known equilibrium by $\alpha = \alpha_{known}(p'/p'_{known})(I_{p,known}/I_p)^2$). Since the major and minor radius changes very little in JET experiments, we used the geometric factors (in ∇r) from the known equilibrium as well. We call this model "stand-alone", as it uses the known temperature to distinguish it from the

full Europed modelling where the temperature profile is also predicted.

We test the model with and without the KBM contribution to D_{ped} and vary $(D_e/\chi_e)_{ETG}$. Figure 1 shows the predicted density against the experimental density when $C_{KBM} = 0$. It can be seen that, if the KBM transport is ignored, the ETG particle transport has to be increased to a level ($(D_e/\chi_e)_{ETG} = 0.5$) that is significantly higher than is expected for ETG modes [7]. It must be noted that even in this case the experimental trend is reproduced (RMSE=20%).

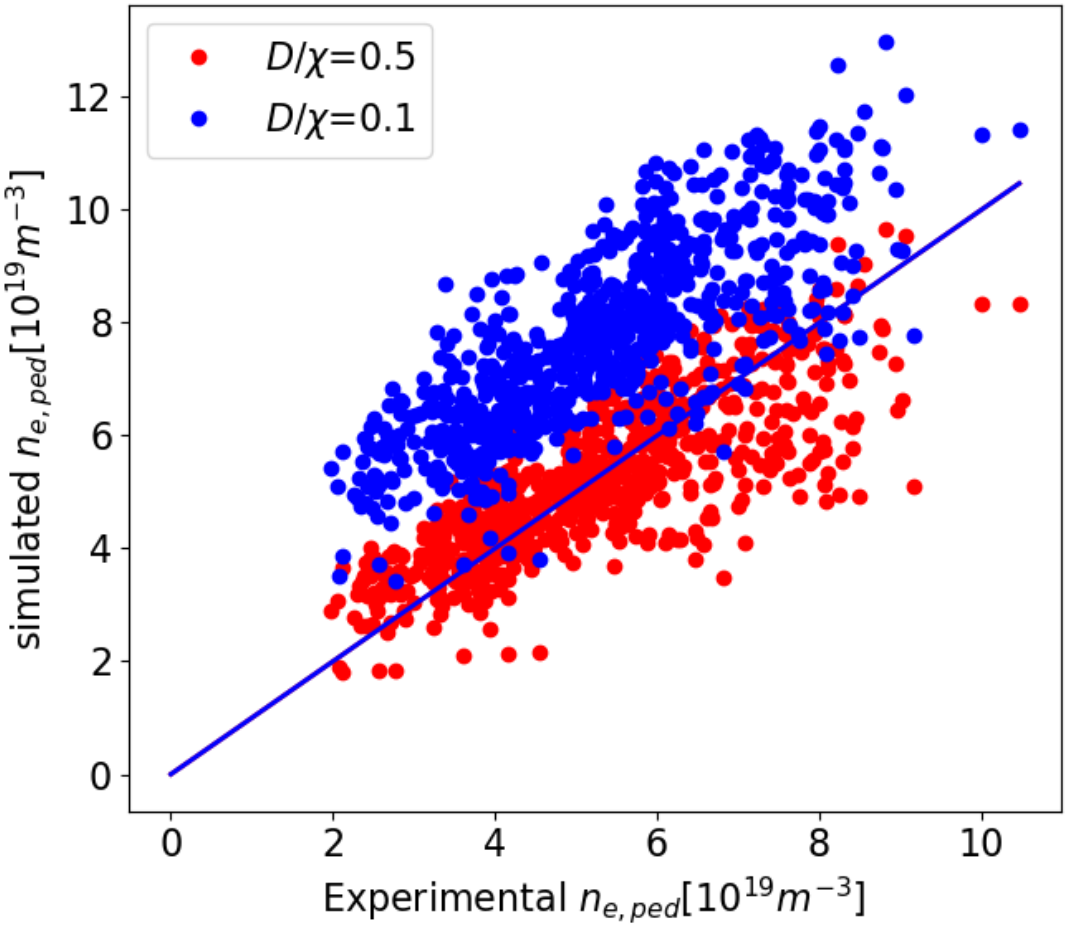

Figure 1. The testing of the standalone pedestal density modelling against the experimental pedestal density using the ionization model ignoring the KBM transport for two values of

$(D_e/\chi_e)_{ETG} =$ 0.5 (red) and 0.1 (blue). The blue line represents the perfect prediction.

The ideal MHD $n = \infty$ ballooning mode limit in JET geometry is at about $\alpha = 3$. Taking into account that the KBM limit is generally lower than that of the ideal MHD limit and that we are using the average value in the pedestal, we use $\alpha_{\mathrm{crit}} = 2$ in the D_{KBM} model, expression (22). Based on the considerations in Ref.7, we choose C_{KBM}= 0.3 but recognize that the model is not very sensitive to this value, provided it is sufficiently large that the main effect of the KBM transport is to force the pedestal pressure gradient to be close to the KBM limit.

Figure 2 shows the model results for two values of ETG particle transport, $(D_e/\chi_e)_{ETG} =$ 0.5 and 0.1. When compared to Fig. 1, we can see that the $(D_e/\chi_e)_{ETG} =$ 0.5 case is hardly affected, meaning that most of those cases were below the KBM limit already. The $(D_e/\chi_e)_{ETG} =$ 0.1 case is strongly affected, matching much better with the experimental values. We obtain very good agreement between the model and experiment for both cases (the RMSE = 17% for $(D_e/\chi_e)_{ETG} =$ 0.1 and the RMSE = 15% for $(D_e/\chi_e)_{ETG} =$ 0.5). Increasing C_{KBM} further to 1.0 changes the result very little from Fig. 2, indicating that at sufficiently high C_{KBM} the pedestal α is limited close to the KBM limit.

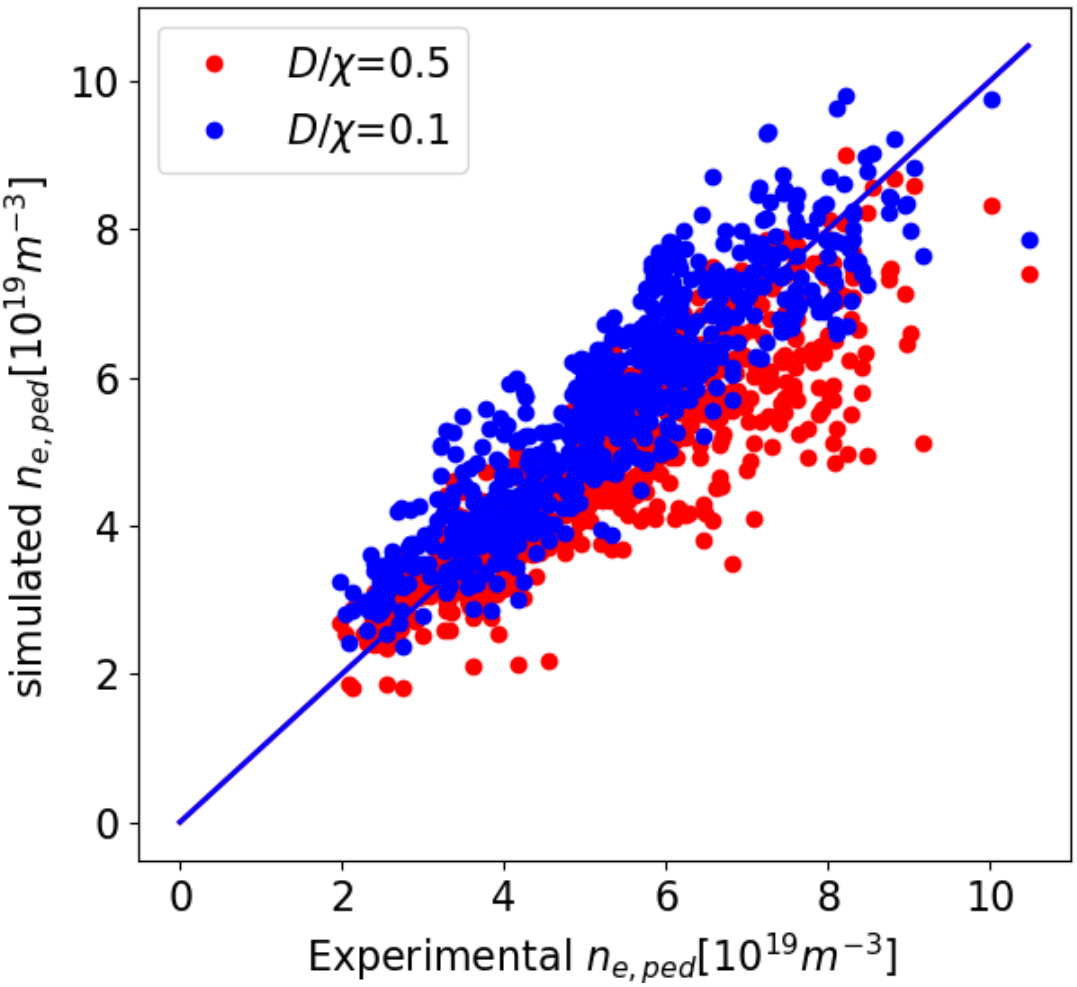

Figure 2. The testing of the standalone pedestal density modelling against the experimental pedestal density using the ionization model with KBM transport (C_{KBM} = 0.3 and $\alpha_{crit} = 2$) for two values of $(D_e/\chi_e)_{ETG} =$ 0.5 (red) and 0.1 (blue). The blue line represents the perfect prediction.

4. Europed Modelling

4.1. *Implementation in Europed*

Europed is an implementation of the EPED model [2] that includes several extensions outlined in Ref.15. The EPED model predicts the pedestal plasma profiles given a set of input parameters (plasma

shape, toroidal field, plasma current, global β, pedestal and separatrix densities). Most of them can be known in advance of the experiment. However, β, pedestal and separatrix density are not necessarily known. The Europed extensions in Ref. 15 tried to predict these values by using inputs such as heating power and fuelling rate. While the results were encouraging, the model for the density pedestal prediction was very specific for JET and most likely does not generalize to other tokamaks. Further, it produced the opposite dependence on the isotope mass from what was seen in the experiment.

Therefore, in this work it is replaced with the model outlined above. In the full model, the density prediction is combined with the EPED constraint $\Delta = c\sqrt{\beta_{p,ped}}$, where Δ is the width of the pedestal, c is a constant (c = 0.076 in the EPED1 model) and $\beta_{p,ped}$ is the poloidal β at the top of the pedestal. This constraint is used to calculate the temperature pedestal for given Δ and the corresponding density pedestal calculated by the ionisation model described above. In practice this is implemented by iterating between the calculation of density profile using a known temperature profile as in Section 3 and calculating the temperature pedestal profile using the EPED constraint. Finally, the peeling-ballooning stability calculation is used to select the pedestal that is marginally stable as the final prediction. In the density model of Europed, we use the same parameters as in the stand alone model. We also test the sensitivity of the model results to the input parameters. The modelling is done in a similar manner to Ref.15, except that we use the new bootstrap current model by Redl introduced in Ref.16 that is shown to work better than the Sauter model used in Ref.15 at high collisionality, but it was not available when the modelling of Ref.15 was done.

4.2 Europed Results

We first test the model without the KBM particle transport (i.e., $C_{KBM} = 0$). Using the value of $(D_e/\chi_e)_{ETG} = \ 0.5$, we obtain the

result shown in Fig. 3 with RMSE = 20%. The scatter of the data is slightly worse than with the standalone model that uses the experimental temperature profile.

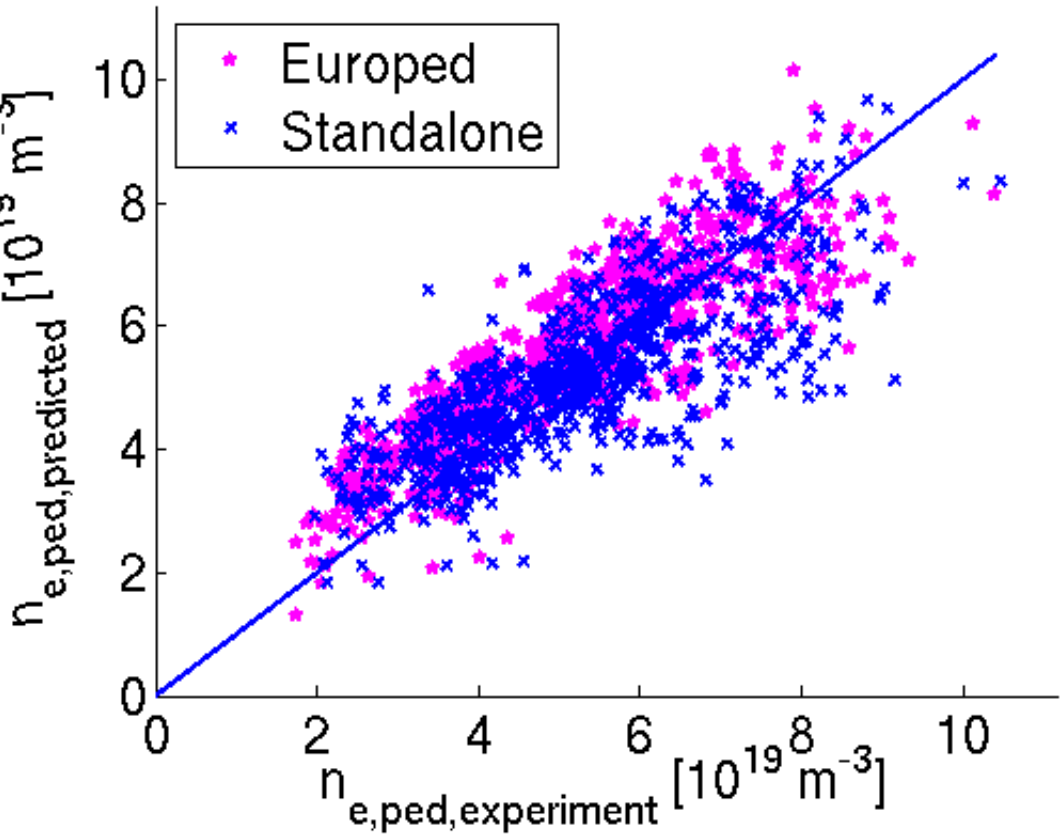

Figure 3. The comparison of the prediction of the pedestal density against the experimental pedestal density using the ionization model ignoring the KBM transport and assuming $(D_e/\chi_e)_{ETG} = 0.5$ *for the full Europed modelling (magenta) and standalone model with experimental temperature (blue). The blue line represents the perfect prediction.*

Next, we include the KBM transport and decrease the ETG particle transport, which was found to improve the fit in the standalone model. We use the following parameters $\alpha_{crit} = 2$, $C_{KBM} = 0.1, (D_e/\chi_e)_{ETG} = 0.2$. Unlike in the standalone model, with the full Europed model we get a worse match with the experiment, as shown

in Fig. 4. In particular, the low experimental values of $n_{e,ped}$ are under predicted This is the case, despite the Europed modelling being performed with a relatively modest KBM transport assumption, compared to what was used with the standalone model.

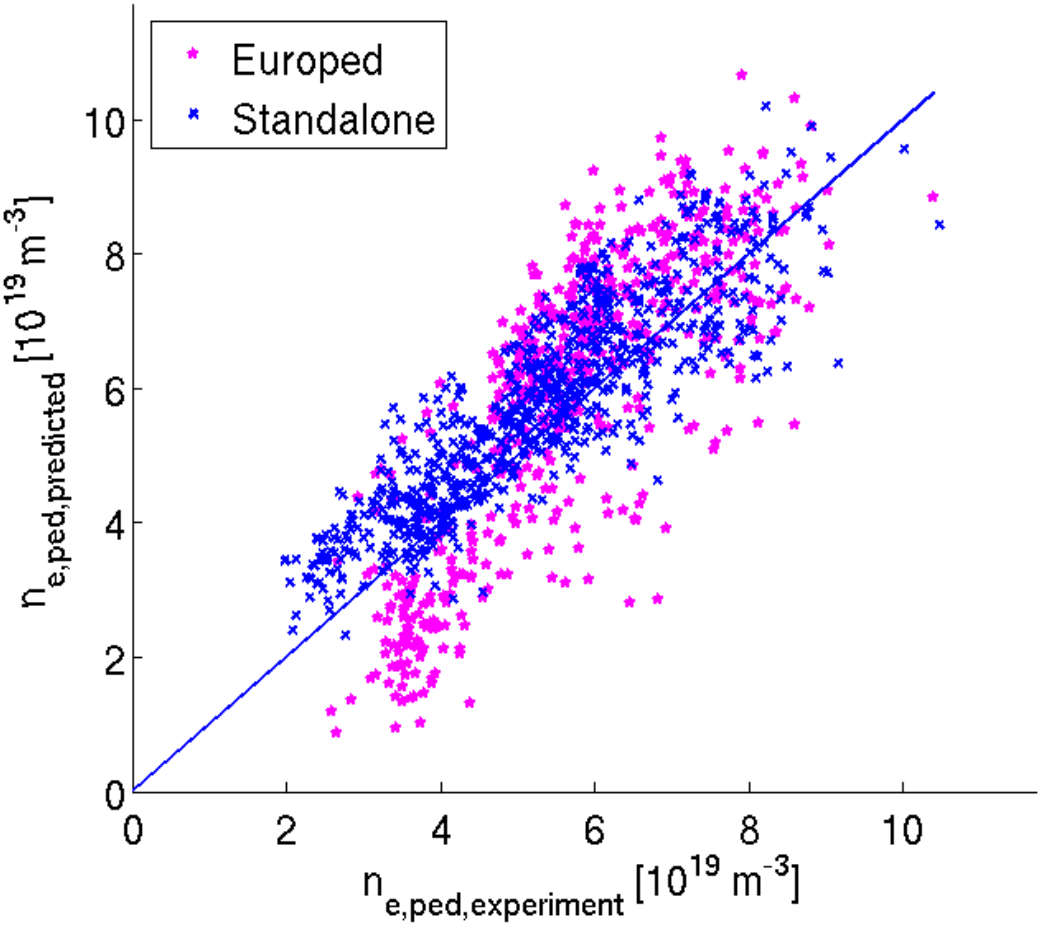

Figure 4. The comparison of the prediction of the pedestal density against the experimental pedestal density using the ionization model including the KBM transport with the parameters $\alpha_{crit} = 2$, $C_{KBM} = 0.1$, $(D_e/\chi_e)_{ETG} = 0.2$ *using full Europed (magenta). For comparison the standalone predictions with the same parameters are shown (blue). The blue line represents the perfect prediction.*

The optimal result is achieved with a very small KBM component of the particle transport ($C_{KBM} = 0.05$), combined with a relatively large ETG component ($(D_e/\chi_e)_{ETG} = \quad 0.5$), although the improvement over the modelling without any KBM transport is small (RMSE = 19%).

We compare this final model to the model predictions in Ref.15 that used a simple neutral penetration model:

$$n_{e,ped} = \frac{2V_n}{\sigma_i V_{th,e} E \Delta_{e,ped}}, \tag{25}$$

where V_n is the velocity of the neutrals, E is the flux expansion ratio between the fuelling location and the midplane and $\Delta_{e,ped}$ is the pedestal width, while other quantities are as above. Although in Ref.15 E was found to depend *on triangul*arity, this has little physics basis and was only included as it improved the fit with the experiment. Nevertheless, we compare the new model results with the old model run with $E = 2.41\phi^{-0.2}\delta^{0.53}$ (where ϕ is the gas fuelling rate in units of 10^{22} *electrons/s* and δ is the triangularity).

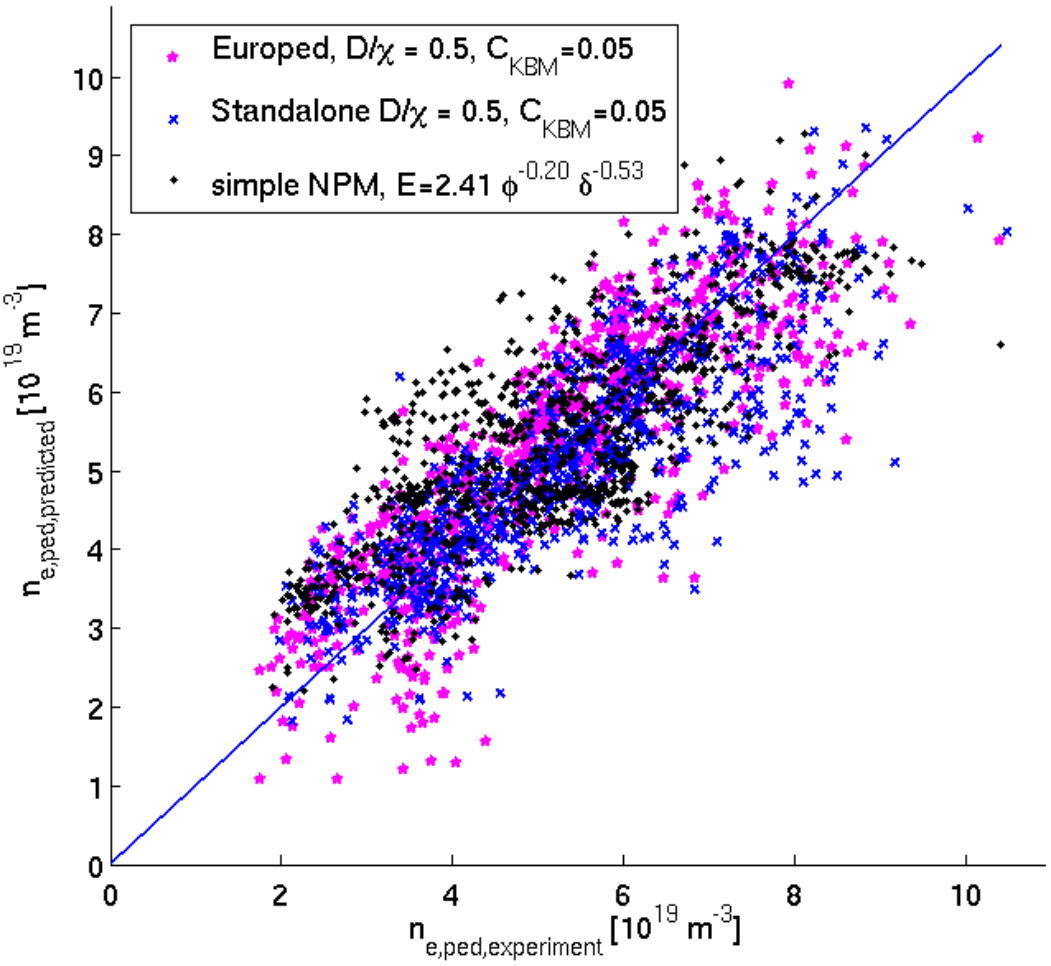

Figure 5. The comparison of the prediction of the pedestal density against the experimental pedestal density using the ionization model including the KBM transport with the parameters $\alpha_{crit} = 2$, $C_{KBM} = 0.05$, $(D_e/\chi_e)_{ETG} = 0.5$ *using full Europed (magenta stars) and the standalone (blue crosses). For comparison the predictions using the simple neutral penetration model in Ref.*15 *are shown (black dots). The blue line represents the perfect prediction.*

As can be seen in Fig. 5, the model performs similarly at medium densities to the model used in Ref.15 which has an RMSE = 25%, but is in better agreement with the experiment, both at high and low density.

The significant difference between the full Europed prediction compared to that of the standalone model is that the fit of the predicted to experimental data is significantly worse when the KBM transport is included than when it is not. Of course, it must be noted here that the model with the fixed α_{crit} value, regardless of, for instance, the role of magnetic shear in the pedestal that has been found to affect KBM stability, may be too crude for this model and a better result could be obtained by using the ideal MHD, $n = \infty$ ballooning mode stability limit as a proxy for KBM stability limit, but that is left for future work.

One explanation for this behaviour of the pedestal density prediction is that the KBM constraint is already included in the EPED model used in Europed. This leads to a feedback loop in the iteration, where the model increases D_{ped} when a particular pedestal exceeds α_{crit}. This leads to a lower density pedestal, which is then compensated in the model by increasing $T_{e,ped}$ (to keep $\beta_{p,ped}$ fixed for the given temperature pedestal width), which then returns the value of the pedestal α to above α_{crit}, and the density is then reduced even further.

This could be avoided in the future development of the model if the EPED criteria for the pedestal pressure is replaced by a criterion for the temperature profile (e.g., $\nabla T/T$ = constant as used in Ref.13) that is independent of the pedestal pressure. Another option is to use a stiff ETG turbulence-based model where $\chi_{ETG} \propto (1 - \eta_e)\nabla T/T$ [7,14], where $\eta_e = (\nabla T/T)/(\nabla n_e/n_e)$. However, this model may suffer the same kind of internal instability as the EPED model as the temperature profile depends on the density profile, which in turn depends on the density profile. Furthermore, it uniquely defines both profiles, which makes the peeling-ballooning constraint irrelevant. A possible way to include it would be to make $n_{e,sep}$ the free parameter (similarly to Δ in the EPED model) and choose the

pedestal profile associated with the value of $n_{e,sep}$ that corresponds to marginal stability.

4.3 Sensitivity of the model

While the model is able predict the experimental behaviour remarkably well when using experimental parameters, it still has some sensitivity to the input parameters that are not known before the experiment; in particular, the separatrix density used for the boundary condition for the prediction model can strongly affect the pedestal density prediction. Figure 6 shows the dependence of the pedestal density prediction on the separatrix density for a sample case where the experimental pedestal density was predicted accurately. Since the pedestal density prediction is so sensitive to the separatrix density, the predictions using this model should be integrated with a full scrape-off layer model or at least with a simple separatrix density model such as that used in Ref.13, where the separatrix density is connected to the neutral pressure at the divertor, which in turn can be calculated from the known gas fuelling rate, heating power and divertor pumping speed. However, this method may not work for a device for which we have no prior data (such as ITER), in which case the only option is the full scrape-off layer modelling. It must be noted that since the gas fuelling rate can be adjusted during the experiment, $n_{e,sep}$ may not have to be fully predicted but can be adjusted to a desired value with a feedback system to a gas fuelling system.

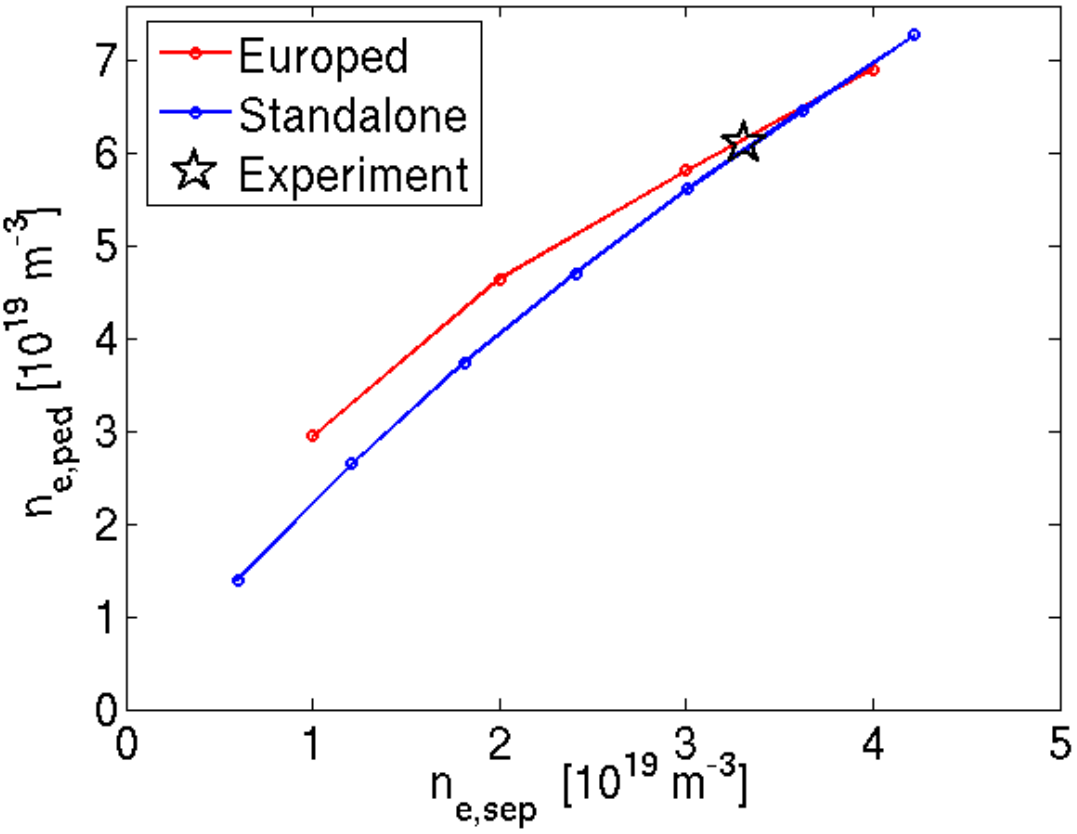

Figure 6. The pedestal density prediction as a function of assumed separatrix density using the standalone model with the experimental T_e profile (blue) and the full Europed model (red). The star represents the experimental case.

The other parameter in the model that we need to make assumptions about, is the Franck-Condon neutral density at the separatrix, $\langle n_{FC}(0) \rangle$. Figure 7 shows that the model is relatively insensitive to this parameter and an order of magnitude change from $10^{15} m^{-3}$ to $10^{16} m^{-3}$ in $\langle n_{FC}(0) \rangle$ changes the $n_{e,ped}$ prediction only by about 20% in the full Europed simulation. We can also see that the dependence of $n_{e,ped}$ on $\langle n_{FC}(0) \rangle$ is linear in both the standalone and Europed models.

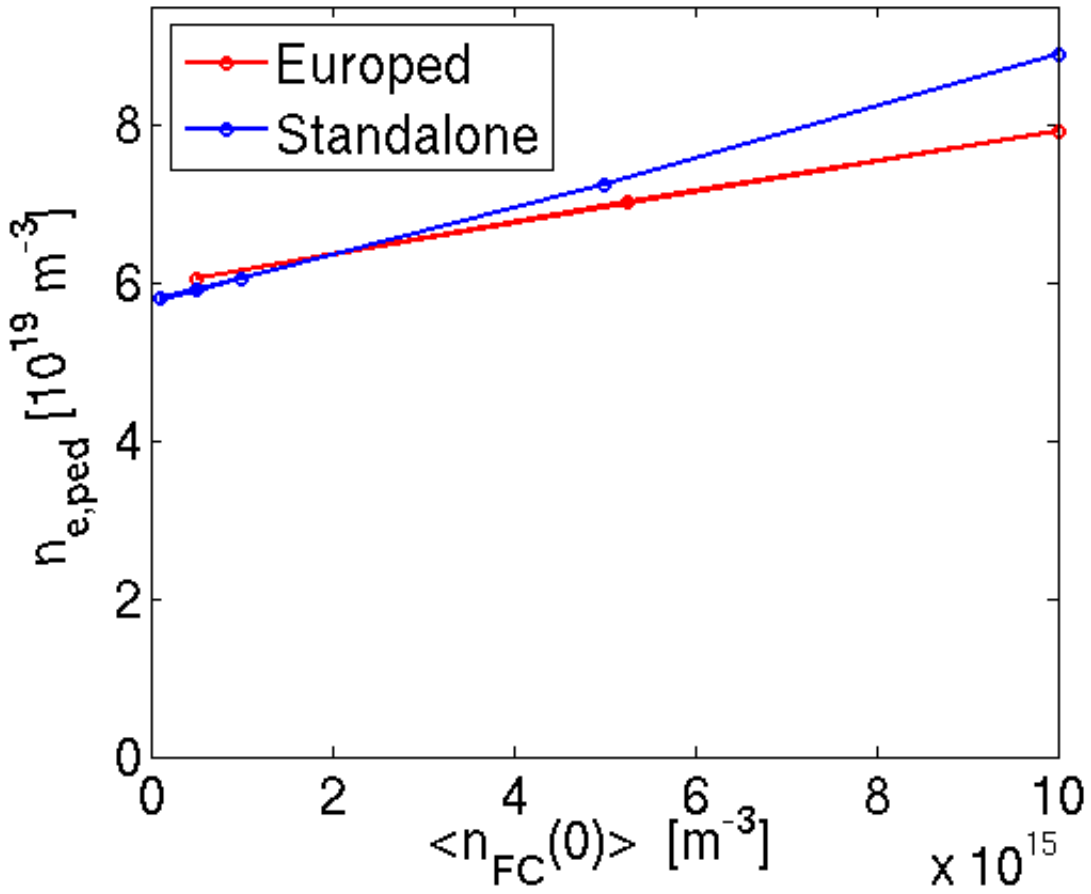

Figure 7. The pedestal density prediction as a function of assumed Franck-Condon neutral density at the separatrix $\langle n_{FC}(0) \rangle$.

5. Isotope effect

In the JET experiments it has been found that with a similar gas rate and heating power, the plasmas with hydrogen have lower pedestal density than those with deuterium [17]. In the model presented in this paper, the isotope mass enters explicitly only through the velocity of the neutral particles (V_{FC} and V_{CX}). As both are $\propto 1/\sqrt{m_i}$, they are higher for hydrogen than for deuterium. The ion mass effect can be investigated by running Europed with the density prediction model and changing only the main ion mass in the simulation for a hydrogen plasma (JET-ILW discharge #91554). This result is shown in

Fig. 8. As expected, the change of the isotope from hydrogen to deuterium while keeping everything else fixed decreases the pedestal density prediction. However, the change of the isotope mass is not the only thing that changes in the JET experiment. In addition, the separatrix density is lower in the hydrogen than in the deuterium experiment [17]. As shown in Fig 8. when we use the $n_{e,sep}$ from the deuterium case that was performed with the same power (84796), the predicted $n_{e,ped}$ increases by more than what the pure isotope effect causes. Both the deuterium and hydrogen cases are well predicted when the experimental $n_{e,sep}$ is used. This is because the model is sensitive to $n_{e,sep}$, with the prediction of $n_{e,ped}$ decreasing with decreasing $n_{e,sep}$.

Furthermore, to reach the same value of global β, more heating power is required in the hydrogen plasma [17]. This means that with the same global β the hydrogen plasma will have a larger value of χ_{ETG} in the model, and even with a fixed value of the $(D_e/\chi_e)_{ETG}$ ratio, the particle transport in the model increases with increased heating power, which in turn leads to a lower predicted $n_{e,ped}$ in hydrogen. If the (D_e/χ_e) ratio also increases as suggested by the EDGE2D-EIRENE modelling in Ref. 17, this further lowers the predictions in hydrogen.

We ignore the possible increase of the $(D_e/\chi_e)_{ETG}$ ratio but use the experimental $n_{e,sep}$ and heating power in the modelling of the hydrogen plasmas. With these assumptions, the hydrogen cases are only slightly over-predicted compared to the deuterium ones. This is shown in Fig. 8 for both the standalone and full Europed models. As can be seen, both the experimental and predicted $n_{e,ped}$ are lower for the hydrogen plasmas than in the deuterium plasmas. The RMSE is 32% for the standalone and 38% for the Europed predictions for the hydrogen plasmas. Finally, on doubling $(D_e/\chi_e)_{ETG}$ (black points

in Fig. 9) the models predict the hydrogen cases with RMSE = 19% (standalone) and 27% (Europed).

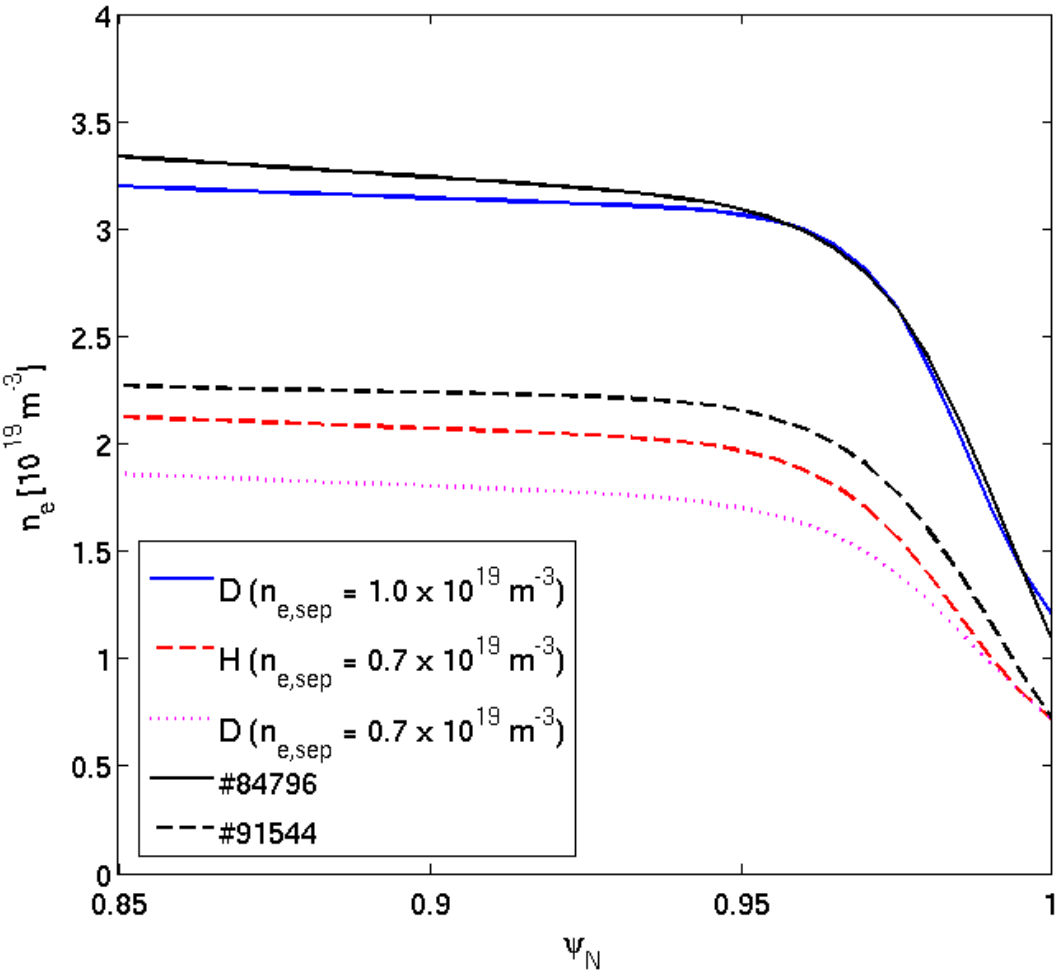

Figure 8. Europed predicted density profiles for JET-ILW discharge 91554 assuming $n_{e,sep}$ from the experiment and hydrogen plasma (dashed red), $n_{e,sep}$ from the experiment and deuterium plasma (dotted magenta), $n_{e,sep}$ from the equivalent deuterium discharge, 84796 and deuterium plasma (blue solid) and the profile from the experiment (91554, black dashed, 84796 black solid).

a)

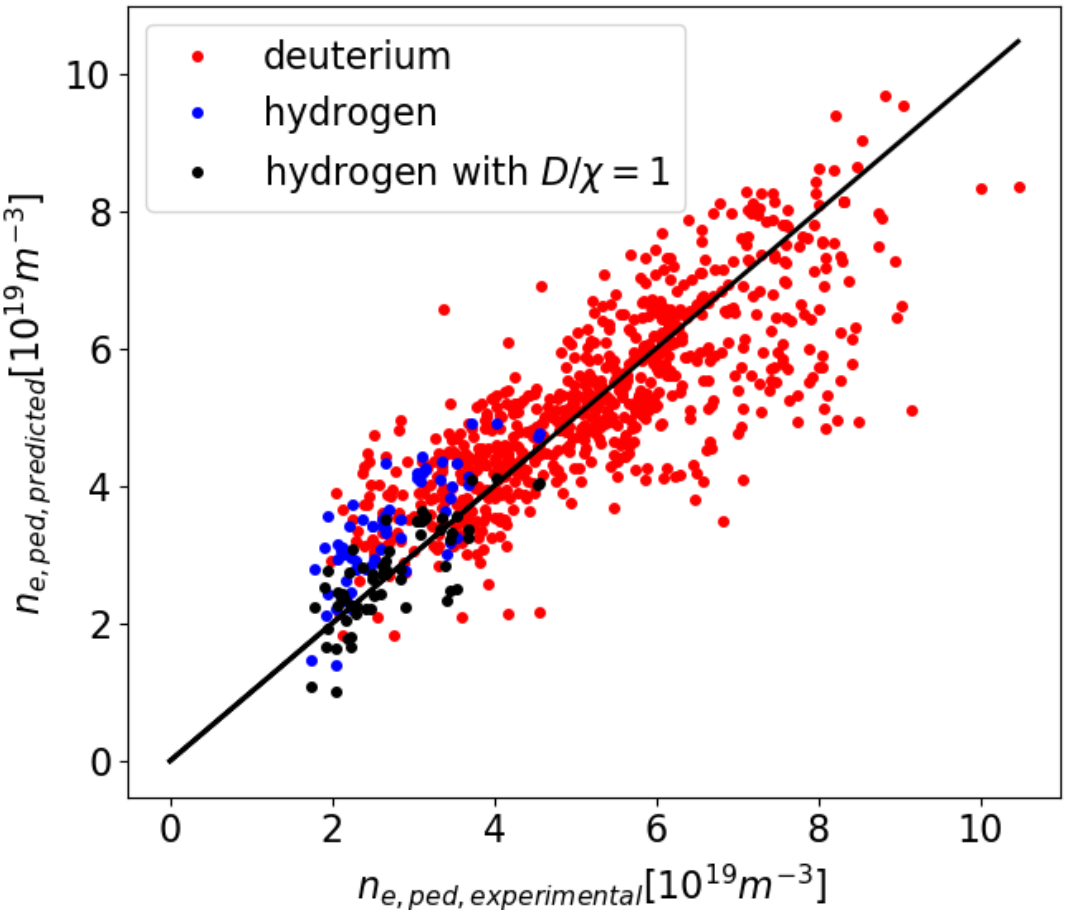
deuterium
hydrogen
hydrogen with $D/\chi = 1$
$n_{e,ped,predicted}[10^{19}m^{-3}]$
$n_{e,ped,experimental}[10^{19}m^{-3}]$
0
2
4
6
8
10

b)

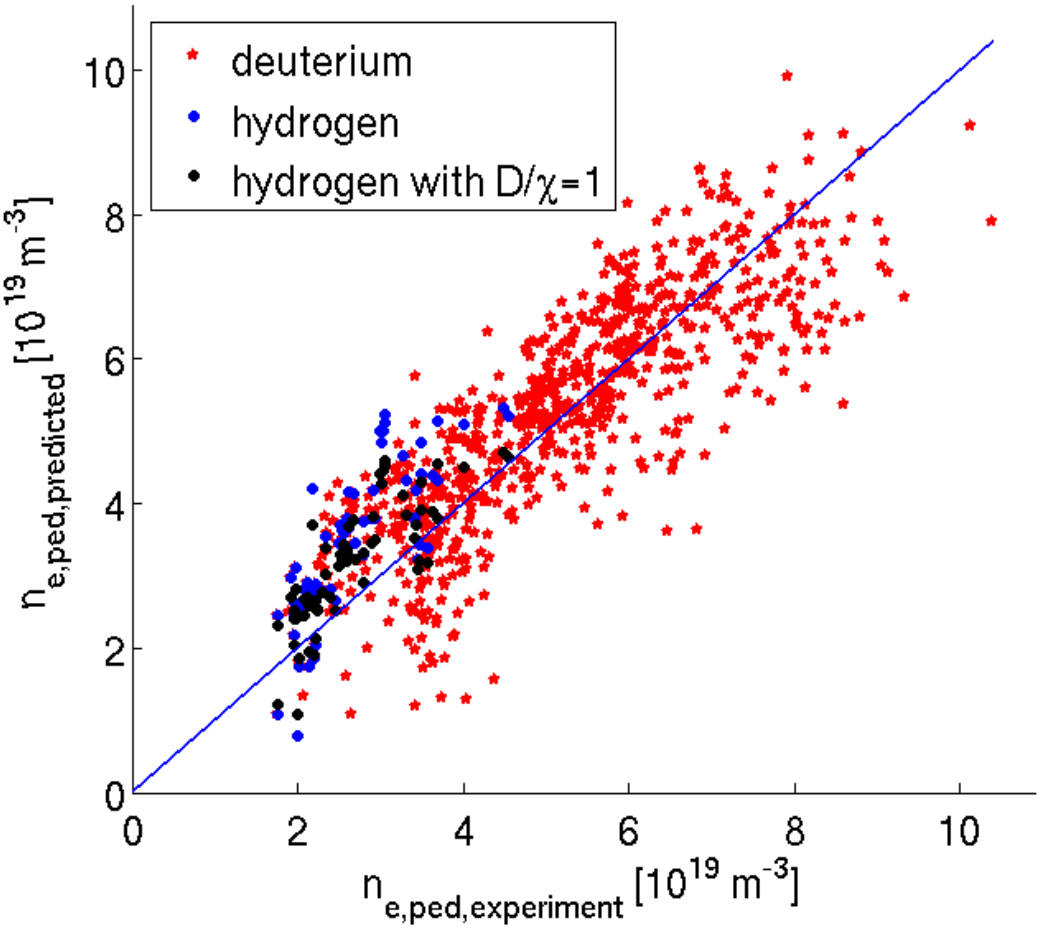

Figure 9. The predicted pedestal densities using the standalone model with experimental temperature profiles (a) and the full Europed model (b) for deuterium (red) and hydrogen (blue). The model parameters for both isotopes were $\alpha_{crit} = 2$, $C_{KBM} = 0.05$, $(D_e/\chi_e)_{ETG} = 0.5$. *The hydrogen case is also predicted using* $(D_e/\chi_e)_{ETG} = 1$ *(black).*

6. Conclusions

We have extended the ionisation model for the density pedestal presented in Ref. 5 in two ways:

(i) We permit a core density gradient, a more realistic situation, which unfortunately prevents a simple analytic solution of the resulting second order differential equation as presented in Ref.5, so that a numerical solution is required.

(ii) Stimulated by techniques in Ref. 6 we include a self-consistent population of charge exchange neutrals. This results in a fourth order system of differential equations, thus requiring four boundary conditions, which can be taken to be the influx of neutrals, the core electron radial density gradient and the pedestal electron density and its gradient. An analytic integration reduces this to a non-linear third order differential equation, but an alternative formulation, an iterative solution to a second order equation, is described.

In addition, we have incorporated the density prediction model as a standalone model, both using experimental temperature profiles and in the Europed approach that predicts both the density and temperature pedestals, with the required particle diffusion coefficient arising from ETG and KBM turbulence. In testing it against the JET-ILW pedestal database, we find:

(i) The full pedestal modelling with the Europed model for the pedestal pressure, reasonable assumptions for the scrape-off layer neutrals and assuming that the particle transport coefficient is tied to the heat transport in the pedestal, can predict the pedestal density for JET-ILW to high accuracy throughout the pedestal database. Including a strong KBM component with the transport increasing rapidly after the stability limit is crossed, gives good predictions with the standalone model, but leads to too much transport in the full Europed model due to the underlying pedestal pressure model that keeps the pedestal pressure gradient fixed for a given pedestal width.

(ii) The density pedestal prediction is sensitive to the boundary condition $n_{e,sep}$, which is not an engineering parameter. This means that for a full pedestal profile prediction, the model needs to be integrated with a scrape-off layer model that can predict the value of $n_{e,sep}$.

(iii) The full model can predict the experimentally observed isotope effect in the pedestal density, even though the isotope effect on the neutral penetration alone is opposite to the observed trend. This is due to the sensitivity of the model to $n_{e,sep}$ as well as the decreasing particle transport in the pedestal with isotope mass.

To further improve the predictive capability of the model presented here requires coupling it with a scrape-off layer model that could predict $n_{e,sep}$ using only engineering parameters such as the divertor configuration and gas fuelling rate. The model should also be tested against experimental data from other devices to determine the robustness of the parameters used in it. An alternative to the EPED modelling of the temperature profiles would be to use a physics-based thermal transport model involving, say, electron temperature gradient and kinetic ballooning modes, together with ion neoclassical transport, thus providing a complete model for predicting pedestal characteristics. pedestal A simpler alternative would be to use stiff transport models for electron temperature gradient and kinetic ballooning modes for the temperature profiles.

Acknowledgements

This work has been carried out within the framework of the EUROfusion Consortium, funded by the European Union via the Euratom Research and Training Programme (Grant Agreement No 101052200 — EUROfusion). Views and opinions expressed are however those of the author(s) only and do not necessarily reflect

those of the European Union or the European Commission. Neither the European Union nor the European Commission can be held responsible for them.

This work has been part-funded by the EPSRC Energy Programme [grant number EP/W006839/1]. To obtain further information on the data and models underlying this paper please contact PublicationsManager@ukaea.uk*.

References

1. A M Dimits, G A Bateman, M Beer, B I Cohen, W Dorland, G W Hammett et al., *Comparisons and physics basis of tokamak transport models and turbulence simulations*, Phys. Plasmas **7** 969 (2000)
2. P B Snyder et al., *Development and validation of a predictive model for the pedestal height*, Phys. Plasmas **16** 056118 (2009).
3. P B Snyder, H R Wilson J R Ferron et al., Phys. Plasmas **9** 2037 (2002)
4. A R Field, B Chapman-Oplopoiou, J W Connor, L Frassinetti, D Hatch, C M Roach, S Saarelma and JET Contributors, *Comparing pedestal structure in JET-ILW H-mode plasmas with a model for stiff ETG turbulent heat transport,* accepted for publication in Phil. Trans. R Soc. A 2022.
5. R J Groebner, M Mahdavi, A W Leonard and T H Osborne et al., *The role of neutrals in high-mode (H-mode) pedestal formation*, Phys. Plasmas **9** 2134 (2002).

6. M A Mahdavi, R Maingi, R J Groebner, A W Leonard et al., *Physics of pedestal density formation and its impact on H-mode density limit in burning plasmas*, Phys. Plasmas **10** 3984 (2003).
7. W Guttenfelder, R J Groebner, J M Canik, B A Grierson, E A Belli and J Candy, *Testing predictions of electron scale turbulent pedestal transport in tokamak DIII-D*, Nucl. Fusion **61** 056005 (2021).
8. M Kotschenreuther, X Liu, D R Hatch, S Mahajan et al., *Gyrokinetic analysis and simulation of pedestals to identify the culprits for energy losses using 'fingerprints'*, Nucl. Fusion **59** 096001 (2019).
9. A Kirk et al., *H-mode pedestal characteristics on MAST*, Plasma Phys. & Control. Fusion **46** A187-194 (2004).
10. C.F. Maggi et al., *Studies of the pedestal structure and inter-ELM pedestal evolution in JET with the ITER-like wall*, Nucl. Fusion **57** 116012 (2017)
11. L Frassinetti et al., *Pedestal structure, stability and scalings in JETILW: the EUROfusion JET-ILW pedestal database*, Nucl. Fusion **61** 016001 (2021).
12. R L Miller et al., *Noncircular, finite aspect ratio, local equilibrium model*, Phys. Plasmas **5** 973 (1998).
13. T. Luda et al., *Integrated modeling of ASDEX Upgrade plasmas combining core, pedestal and scrape-off layer physics*, Nucl. Fusion **60** 036023 (2020).
14. B. Chapman-Oplopoiou et al., *The role of ETG modes in JET–ILW pedestals with varying levels of power and fuelling,* Nucl. Fusion **62** 086028 (2022).
15. S Saarelma et al., *Self-consistent pedestal prediction for JET-ILW in preparation of the DT campaign,* Phys. Plasmas **26** 072501 (2019).
16. A Redl et al., *A new set of analytical formulae for the computation of the bootstrap current and the neoclassical conductivity in tokamaks*, Phys. Plasmas **28** 022502 (2021).

17. L. Horvath et al., *Isotope dependence of the type I ELMy H-mode pedestal in JET-ILW hydrogen and deuterium plasmas*, Nucl. Fusion **61** 046015 (2021).